Digital Signal Processing 55 (2016) 32–43

Contents lists available at ScienceDirect

Digital Signal Processing

www.elsevier.com/locate/dsp

High resolution time-frequency representation for chirp signals using an adaptive system based on duffing oscillators

Antonio H. Costa [a,*], Rogerio Enríquez-Caldera [b], Maribel Tello-Bello [b], Carlos R. Bermúdez-Gómez [b]

[a] Department of Electrical and Computer Engineering, University of Massachusetts, Dartmouth, MA 02747, USA
[b] National Institute of Astrophysics, Optics and Electronics INAOE, Puebla, Mexico

ARTICLE INFO

Article history:
Available online 28 April 2016

Keywords:
Time-frequency
Duffing oscillator
Detection
Estimation

ABSTRACT

This paper presents a novel methodology to estimate the frequency shift in chirp signals with SNRs as low as −17 dB through the use of an adaptive array of Duffing oscillators. The system used here is an array of five Duffing oscillators with each oscillator's response enhanced through a correlation with the reference signal. As a final result, a time-frequency depiction is provided by the Duffing array for further analysis of chirp signals.

Using computer simulated experiments, it is found that the analysis of chirp signals with low SNR by means of the Duffing oscillator shows a markedly better performance than the conventional methods of time-frequency analysis. To this end, the results obtained from the proposed Duffing method are compared against some recent techniques in time-frequency analysis.

Furthermore, to strengthen the proposed representation, Monte Carlo simulation is used.

1. Introduction

Typically, detection and estimation of time-varying signals is done through time-frequency (TF) methodologies like those of short-time Fourier Transform, discrete wavelet transform and other more modern techniques like the Wigner and the Choi–Williams distributions [1]. However, all these TF techniques exhibit difficulties when the time-varying signals under study have low SNRs, as in the case of chirp signals immersed in noise.

In recent years, detection of extraordinarily low SNR signals with a constant frequency has been reported using chaotic oscillators [2–5] and specifically the Duffing oscillator [6–11]. The use of an array of Duffing oscillators has also permitted the detection of nonlinear time-varying frequencies under high levels of noise – with better results than those obtained from conventional TF techniques – working with chirp signals in environments with very low SNRs [12]. This array approach presented a drawback due to its imprecise way of measuring changes in frequency.

In contrast, traditional and modern TF analysis techniques when used to measure signals whose frequency changes over time including the spectrogram, the continuous wavelet transform [13–15] and the Wigner distribution [16–18] have given very accurate results in high SNR scenarios, but they are all seriously impacted when the SNR is too low.

Here, and due to an improvement in measuring and detecting the transitions between the periodic and chaotic states of an array of five, self-adjusting Duffing oscillators, this paper proposes a novel method for the analysis of chirp signals with very low SNR in the TF domain as an advantaged choice to the Choi–Williams distribution [1], and the Multiform Tiltable Exponential Distribution (MTED) [18].

Furthermore, the experimental comparison allowed noticing that there exist two inner limitations related to the Duffing oscillator: i) Despite the published claims that the chaotic oscillator is immune to noise [6,9,11,14,19–23], it has a noise threshold under which the oscillator can work as a good detector; and ii) the array system oscillator also has a measuring threshold for the frequency variation ratio present in the chirp signal.

In what follows, Section 2 provides a short description of the Duffing oscillator chaotic behavior whereas Section 3 describes how such behavior is used to detect chirp signals in high levels of noise and how to obtain the corresponding parameter measurements in the most precise form. Section 4 describes the proposed adaptive system that allows for the measurement of the instantaneous frequency variation of a highly dynamic single component chirp signal within a large frequency range. Finally, Section 5 shows the experimental comparison, based on the relative MSE,

* Corresponding author.
E-mail address: Acosta@umassd.edu (A.H. Costa).

http://dx.doi.org/10.1016/j.dsp.2016.04.008
1051-2004/

among the TF representations using the Choi–Williams distribution, the MTED and the proposed Duffing Adaptive System.

2. Duffing oscillator operation

The general Duffing oscillator can be modeled as the following non-linear differential equation [24]:

$$\ddot{y} + 2\zeta\dot{y} + \mu\dot{y}^3 + \alpha y + \gamma y^3 = 0 \tag{1}$$

where y represents displacement, ζ is the damping ratio, μ is the non-linear damping coefficient, α is the linear stiffness and γ is the non-linear stiffness.

Analysis of the Duffing system under no external force using the homogeneous equation (1) gives 3 equilibrium points, one equilibrium point at $(y_{eq}, \dot{y}_{eq}) = (0, 0)$, and two equilibrium points $(y_{eq}, \dot{y}_{eq}) = (\pm\sqrt{-\frac{\alpha}{\gamma}}, 0)$ under two different conditions [24]:

i) One condition occurs when the stiffness coefficients, both linear and non-linear, have the same sign, that is $\alpha\gamma > 0$.
ii) The other condition occurs when both stiffness coefficients have different signs, that is, $\alpha\gamma < 0$.

Such analysis determines that the Duffing oscillator has a chaotic behavior if and only if all three equilibrium points are present. Further analysis shows that under all the above conditions, the Jacobian evaluated at the corresponding stability points resulted in the non-linear damping element becoming null, that is, $\mu\dot{y}_{eq}^3 = 0$.

Thus, working under such conditions, and when we apply an exciting force composed by the sum of two sinusoidal parts in the presence of additive noise $n(t)$, equation (1) becomes

$$\begin{aligned}&\ddot{y} + 2\zeta\dot{y} - \alpha y + \gamma y^3 \\ &\quad = F_r\cos(\omega t) + A\cos\big[(\omega + \Delta\omega)t + \varphi\big] + n(t)\end{aligned} \tag{2}$$

where F_r is the amplitude of a given single reference signal with the frequency ω chosen to be equal to the initial frequency of an applied input signal (amplitude A, arbitrary phase φ and a frequency drift from the reference of $\Delta\omega$). The additive noise has standard deviation σ.

The operating principle of the oscillator is based on the frequency difference between the two involved signals in the equation: the proper reference signal of the Duffing Oscillator ($F_r\cos(\omega t)$) and the introduced external signal ($A\cos[(\omega + \Delta\omega)t + \varphi]$).

A complete mathematical demonstration of such transitions is developed in [8] where it is also shown that the amplitude of the oscillator's response is given by

$$F(t) = \sqrt{F_r^2 + 2F_r\cos(\Delta\omega t + \varphi) + A^2}. \tag{3}$$

When $F(t)$ is smaller than a given but fixed Fo the oscillator exhibits a chaotic state, and when $F(t)$ is bigger than Fo the oscillator presents its periodic state. Thus, Fo establishes a threshold for transitions between chaos and periodicity [23]. Furthermore, the frequency difference $\Delta\omega$ can be estimated when calculating the time at which those transitions occur by means of

$$\Delta T = \frac{2\pi}{\Delta\omega}. \tag{4}$$

It has also been shown in [20] that any possible noise added to the system, does not affect such transitions and only affects the trajectory of the response, re-enforcing in this manner the chaotic intermittence behavior.

From equation (4), the period at which the transitions occur is inversely proportional to $\Delta\omega$, which allows a precise frequency measurement of the input signal even in the presence of noise. Therefore, measuring the period ΔT is one of the most important steps along the process.

It should be noted that the existing force for this case only contains a single reference signal, thus limiting this development to single component signal applications.

With the purpose of detecting a signal with any frequency variation without necessarily modifying any parameter in equation (1) when ω varies, it is convenient to apply a variable transformation [10] to the system equation, obtaining the state-space system described by

$$\begin{cases}\dot{x} = \omega y \\ \dot{y} = \omega\big(-2\zeta y + \alpha x - \gamma x^3 + F_r\cos(\omega t)\big)\end{cases} \tag{5}$$

It is worth noticing that the state equations (5) have the angular frequency ω as a factor and, therefore, the amplitude in the oscillator response increases as ω increases [4,10,21,23] and this may cause a variation in the threshold between the two possible states. This, in turn, may cause the oscillator to fall off the chaotic intermittence, making it impossible to estimate any dynamic frequency changes in the incoming signal. This has to be taken into consideration when attempting to detect chirp signals.

In other words, frequency measurements work well for stationary frequency signals. However, our motivation is to verify that the Duffing oscillator can permit the measurement of time dependent frequency signals, specifically chirp signals.

3. Chirp detection with the Duffing oscillator

This section is intended to give the reader an idea of how it is possible to detect chirp signals using the Duffing oscillator, the main contribution of this research. We also explain how the system generates a time-frequency representation (TFR). It is important to note here that the proposed system has the ability to detect linear and nonlinear frequency variations and that these variations represent accelerations and decelerations or even changes in acceleration which, in fact, are more consistent with the Doppler Effect in real situations.

The Duffing oscillator working under a reference chirp signal whose frequency variation in time, represented by $\dot{\omega}$, is described by

$$\begin{aligned}&\ddot{y} + 2\zeta\dot{y} - \alpha y + \gamma y^3 \\ &\quad = F_r\cos\big(\omega t + \dot{\omega}t^2\big) + A\cos\big[(\omega + \Delta\omega)t + (\dot{\omega} + \Delta\dot{\omega})t^2 + \varphi\big] \\ &\qquad + n(t).\end{aligned} \tag{6}$$

To work with this type of signal it was assumed that the Duffing oscillator is able to accurately detect the frequency of signals with linear phase variations operating under chaotic conditions as discussed under equation (5). Thus, it is possible to conceive a new time approach where the chirp signal is divided into small time windows short enough to assume that, within each window, the frequency can be considered constant. Furthermore, the selection of the time window has to ensure that the variation of frequency does not take the oscillator out of the intermittence condition.

To calculate the accepted frequency variation present in a windowed linear chirp signal described by

$$X(t) = \begin{cases}\cos(\omega t + \dot{\omega}t^2) & \text{for } t < |\frac{T}{2}| \\ 0 & \text{otherwise}\end{cases} \tag{7}$$

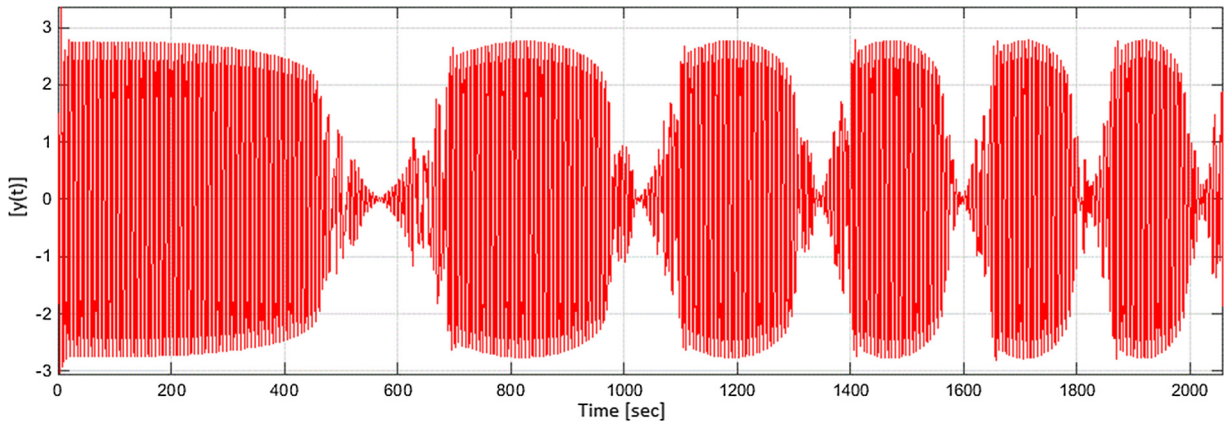

Fig. 1. Oscillator response with chirp reference signal and a frequency variation ratio ω' equal to 0.0001 rad/s^2.

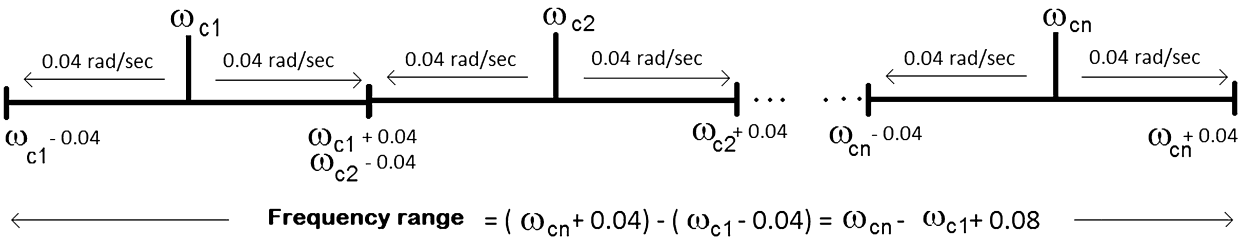

Fig. 2. Array of Duffing oscillators.

where T is the width of a symmetric window in the time domain, let us start with rewriting equation (7) as

$$\cos\left(\omega t + kt^2\right) = \cos(\omega_0 t)\cos\left(kt^2\right) - \sin(\omega_0 t)\sin\left(kt^2\right) \tag{8}$$

where k is the corresponding rate for $\dot{\omega}$.

If kt^2 is small, we get

$$\cos\left(\omega t + kt^2\right) = \cos(\omega_0 t) - kt^2\sin(\omega_0 t). \tag{9}$$

Using Taylor's residue theorem for an expected error of 1%, the value for k can be easily calculated, obtaining $kt^2 = 0.14$ rad for $t < |\frac{T}{2}|$.

Fig. 1 displays the time system response where it is possible to observe the transitions between the chaotic and the periodic states. One drawback is the effect of having two implicit variables in time, namely the difference in speed and acceleration of the chirp signal at which those transitions occur, thus preventing the measurement of $\Delta\omega$ and consequently any changes in acceleration in the signal separately. Furthermore, as it was pointed out in [12], any dynamic changes in frequency cannot exceed 0.04 rad/sec since it is difficult to perceive the intermittent chaos as the transitions occur very rapidly. Hence, it is highly recommended to keep measuring signals where $\Delta\omega < |0.04|$.

Thus, the proposed system would use rectangular time windows in a similar way as in the short-time Fourier transform (STFT) but, in contrast, it does not apply the Fourier transform to each window, but rather each time window is analyzed using an array of Duffing oscillators for as many different frequency references as those that are meant to be detected. Fig. 2 depicts the actual time windowing applied to an incoming signal to a set of Duffing oscillators.

Specifically, each one of the windows dividing the signal is introduced to an array of Duffing oscillators which detects the frequency in the window or, in other words, the instantaneous frequency in the period of time defined by that window.

Fig. 3 illustrates how the frequency measuring procedure is performed for a given initial signal $X1(t)$ – which is the result of

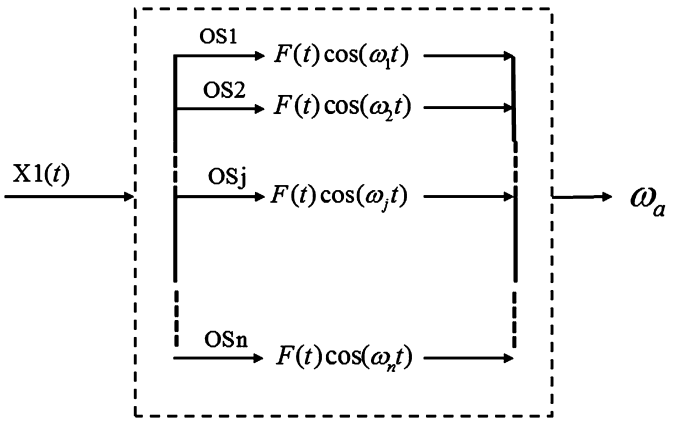

Fig. 3. Array of oscillators analyzing the windowed signal $X1(t)$.

multiplying the incoming signal by the very first rectangular window and later simultaneously introduced to each oscillator OSj in the array. Each oscillator generates transitions between chaos and periodicity as it was expected. Since the oscillators are located at different reference frequencies, each one of them presents a different response, but it must be consistent with the detected frequency by the other oscillators.

To implement such proposed technique, an array of Duffing oscillators is set up where each element OSn of the array gives an estimation of the frequency that is being analyzed for a given time window. The array gives a set of different frequency estimates and at the end an average frequency ω_a is obtained. This procedure is performed for every one of the subsequent time windows that divide the original signal.

3.1. Measurement of $\Delta\omega$

To properly describe the method to detect chirp signals being proposed here, let us assume that there are only 5 Duffing oscillators (OSj, $j = 1, \ldots, 5$) in the array and that the incoming linear

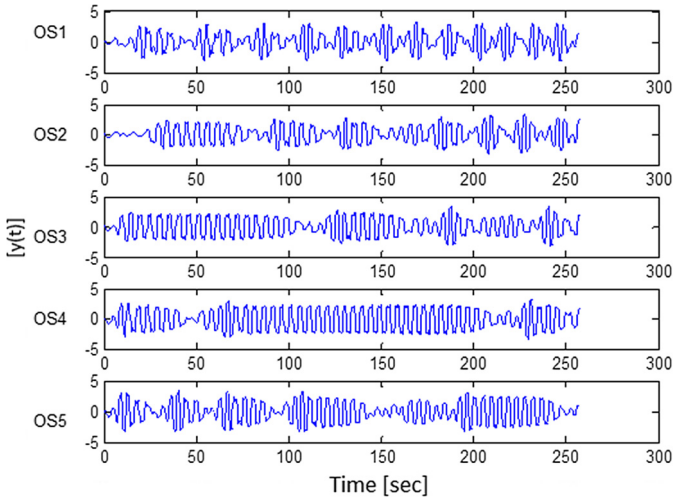

Fig. 4. Response of an array with five Duffing oscillators; spacing among oscillators 0.1 rad/s within the same time window.

chirp signal varies in frequency from 1 rad/s to 1.4 rad/s. Further, and just for the sake of a clear explanation, let us consider a noiseless incoming signal.

For a given time window that is presented to the array, Equation (4) indicates that in order to calculate $\Delta\omega$, it is necessary to measure the time interval Δt at which each oscillator gets in and out of its corresponding chaotic state. Fig. 4 shows that each oscillator generates a signal response with a different period Δt. Thus, there are 5 measurements, which are close to each other, representing different points of reference and permitting us to obtain a very accurate estimate of the actual frequency.

To start measuring Δt, there are some practical considerations based on Fig. 4.

First of all, it is clearly seen that the periodic state on the Duffing oscillator response presents a bigger amplitude than the chaotic state. Thus, it is easy to define an amplitude threshold to properly distinguish the time separation between the points that reach that threshold. Therefore, the first step is to detect the points where the signal has an amplitude above such threshold followed by finding the time region where there exist periodic states. The second step is to identify which points belong either to the same periodic state or to a different one. Once we have identified the points belonging to different periods, the distance Δt between them needs to be measured. However, within the response of the particular oscillator under study, we will find several transitions and very likely the measurements will give different Δt but, still very close to each other. Therefore, all those values are averaged producing the final ΔT for that specific oscillator.

Secondly, from Fig. 4 it can also be easily seen that the OS4 oscillator is the one with the fewer number of transitions and, in agreement with equation (3), that oscillator is at the non-chaotic state. Therefore OS4 is the one that contains the reference closest to the instantaneous frequency of the incoming signal and it should be taken as an adequate estimate of such frequency.

Thirdly, to obtain the most accurate measurement of ΔT, the oscillator with the greatest number of transitions should be taken. Fig. 4 shows that such oscillator is the farthest one from the instantaneous frequency. Precaution should be taken when the number of transitions is so large that it would make it impossible to distinguish one transition from another which, in turn, would make the calculation of $\Delta\omega$ very difficult.

Finally after finding the most precise ΔT, then $\Delta\omega$ can be calculated giving the best estimate of the frequency variation between the reference signal and the incoming signal. Despite having a precise measurement of $\Delta\omega$, such value does not say anything about how the real frequency is changing in time in the sense of not knowing if it increases or decreases; it only says how far away the real frequency from the reference frequency is. Thus, at the moment of calculating the signal frequency, we must consider the reference frequency in the oscillator, aiming to either add or subtract $\Delta\omega$ as appropriate.

To overcome this difficulty, it would be sufficient to observe where the other oscillators are located with respect to the one that gave the proper estimate of the incoming signal. In the case of Fig. 4, the oscillators OS1, OS2 and OS3 are located at a smaller frequency than OS4 and therefore we must add the $\Delta\omega$ to their reference frequencies. Correspondingly, for OS5 the $\Delta\omega$ must be subtracted because it is located at a higher frequency than the OS4 oscillator.

In this way, the proposed array gives us the required information about $\Delta\omega$ because it is possible to identify if it is negative or positive. That is an important reason for applying a Duffing oscillator array.

To conclude, once the frequency is calculated for each oscillator, we can now get the average frequency for all responses. This will be the result generated by the oscillators array and hence would be the most precise estimate of the frequency for the particular time window being analyzed.

The implementation algorithm is as follows:

i) The incoming chirp signal immersed in noise is previously divided into n time windows depending on both the total duration of the whole signal and the condition that the variation of frequency does not exceed the limit of being considered constant for the specific desired precision.
ii) Give a first estimate for the incoming frequency signal and set each of the Duffing local reference frequencies, adjusted within a close variation.
iii) Select the jth oscillator response and identify points above a given amplitude threshold that distinguishes chaos from periodicity.
iv) Account for the i-number of transitions present in the response.
v) Measure Δt_i between all different periodic states.
vi) Calculate the average ΔT.
vii) Perform the same procedure for all Duffing oscillators in the array.
viii) Identify the oscillator with the least amount of transitions and use its ΔT to calculate the better frequency estimate for this observation window.
ix) Decide whether $\Delta\omega$ implies if the frequency is increasing or decreasing.
x) Provide the actual frequency estimate for this window.

The full algorithm is summarized in Fig. 5.

3.2. Signal detection enhancement

Measuring Δt in the Duffing oscillator response is a key process in the system's performance since it is at this point that the detection of the frequency signal takes place. Therefore, it is necessary to estimate Δt with the least possible error to achieve greater accuracy in the measurement.

In this process, it is necessary to identify or highlight any of the two states – periodic or chaotic state – in the oscillators' response to measure the period at which the transitions occur. In the presence of noise, it is observed that the difference in amplitude between the periodic and chaotic oscillator becomes less distinct, as seen for all OSj, $j = 1, 2, 3, 4, 5$, in Fig. 6.

For this reason, it is critical to study different methodologies that highlight some of both states to improve measurements

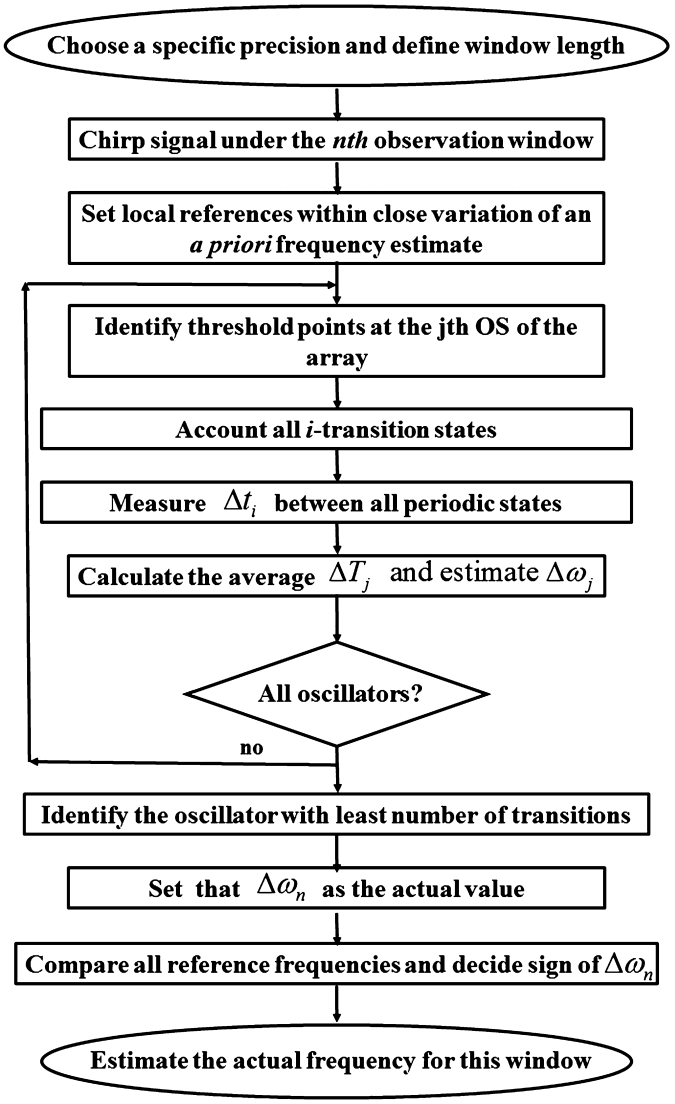

Fig. 5. ΔT measurement and estimation of the actual window frequency.

and thus, introducing in the system a process to enhance chaos-periodicity transitions.

Fig. 7 shows how the whole process is modified for a better frequency estimate from the Duffing oscillator array.

In Fig. 7, $y(t)$ is the Duffing oscillator response and $s(t)$ is the new signal that is used to measure ΔT.

The *signal enhancement* block is responsible for improving the oscillator response in order to identify the transitions between the states with better accuracy. The studied methods for this purpose were:

a) Melnikov Function [8,21].
b) Lyapunov Exponent [11,22].
c) Correlation [25,26].
d) High Order Cumulants [27–29].
e) Squared Response [12,20] of the Duffing Oscillator.

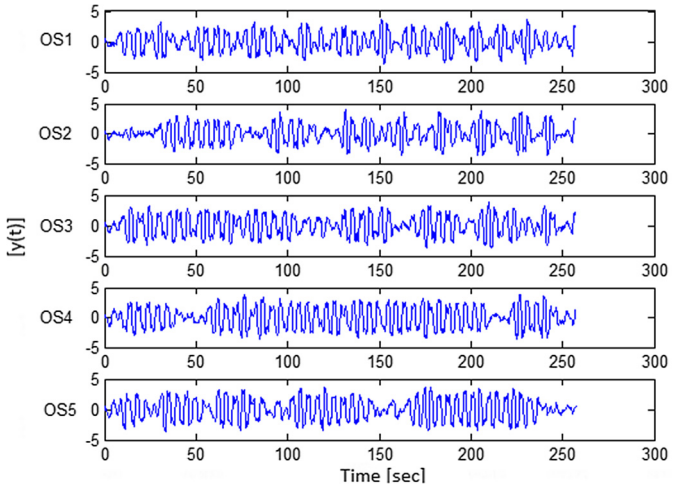

Fig. 6. Response of an array of 5 oscillators with −10 dB of SNR, spacing 0.1 rad/s among oscillators within the same time window.

Fig. 8 shows the results of applying all these methodologies to enhance the signal.

The enhancement process is described in [30] and concluded that the correlation method permits the improvement of frequency measurement up to a limit of −28.5 dB of SNR with good accuracy. This fact is confirmed directly in Fig. 8 and, therefore, such method was selected and used by the entire system.

In scenarios with very high levels of noise, a problem may persist when measuring the different ΔT_j which consists in that sometimes there is a periodic state that fails to overcome the previously selected threshold amplitude. For the example in Fig. 6, the problem occurs within the OS5 oscillator at the particular 5th transition. One can see that this periodic state has a lower amplitude than the others.

To solve this situation, the method for the ΔT_j estimation performs a measurement of distances between each of them and compares with the average of the entire signal to later make an automatic assignment of the points that are needed.

4. Adaptive system

An inherent difficulty in the array of Duffing oscillators is that in order to use a chirp signal as a reference, it would be necessary to know beforehand the signal to be measured and to adjust the frequency and acceleration parameters accordingly or, at least to know if the frequency rate of the incoming signal is of second order or higher. Hence, the system is rendered useless when measuring a signal that could have unknown variations in frequency.

The Duffing array provides a larger frequency range than a single Duffing oscillator because the whole chirp signal is broken in a set of time windows. However, although the use of an array of oscillators produces very good frequency estimation of the signal, it has limitations for detecting the instantaneous frequency in a signal whose frequency range is broad. This could happen because of the possible existence of very high dynamics involved in the given chirp signal. One way of widening the frequency range is to have a very large array of oscillators.

The described procedure in the previous section shows that the arrangement of 5 oscillators works very well because it is easy to

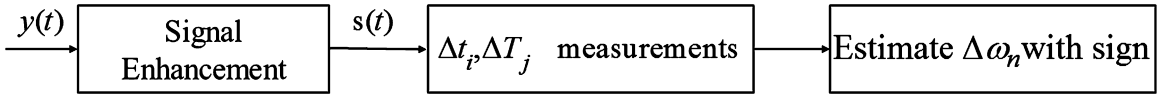

Fig. 7. Frequency estimation enhancement from the Duffing oscillator response.

precisely measure ΔT but, when the array is large, the oscillators that are located too far from the actual instantaneous frequency could not perform an accurate measurement of frequency due to the sensitivity of working in chaotic intermittence.

To avoid the use of a large array of oscillators, we also propose a practical solution that consists of generating a system array able to recursively follow the instantaneous frequency detected in a chirp signal. This means that the array adjusts itself to the changes in frequency of the incoming signal independently of those changes increasing or decreasing the frequency.

The proposed operating principle is based on the following: after obtaining a first estimate of the instantaneous frequency (using a small window analyzed by the 5 oscillators as described above) then, for the next window that is going to be analyzed, the local reference frequency for each of the oscillators is adjusted according to that specific value. This procedure repeats itself for the whole duration of the incoming signal and so ensures that the array of oscillators is always close to the instantaneous frequency of the chirp signal.

This method is always going to need a fixed number of oscillators regardless of the frequency range. In addition, because

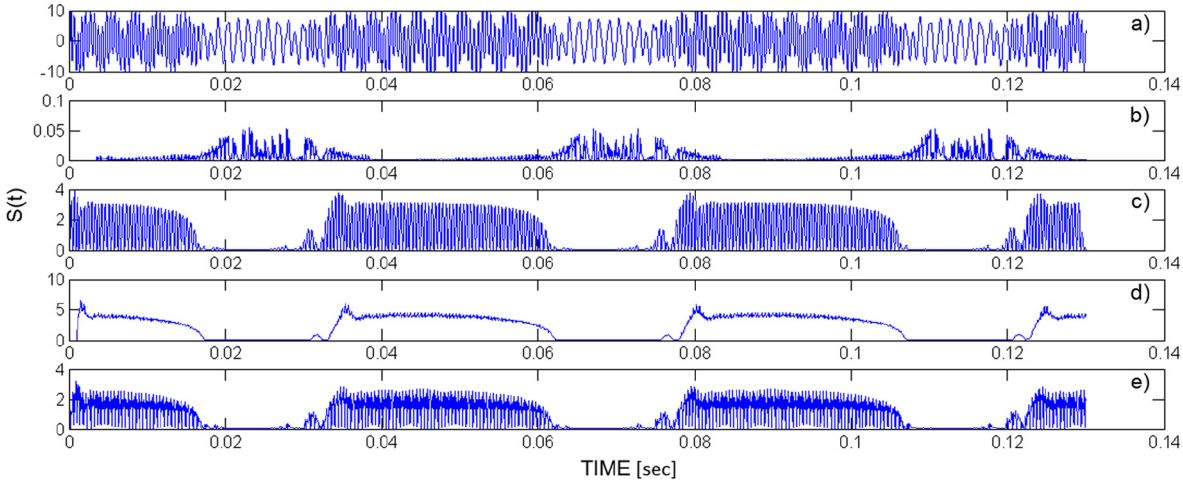

Fig. 8. Comparison of signal enhancement methodologies: a) Melnikov function, b) Lyapunov exponent, c) Correlation, d) 4th order Cumulant, and e) Squared signal.

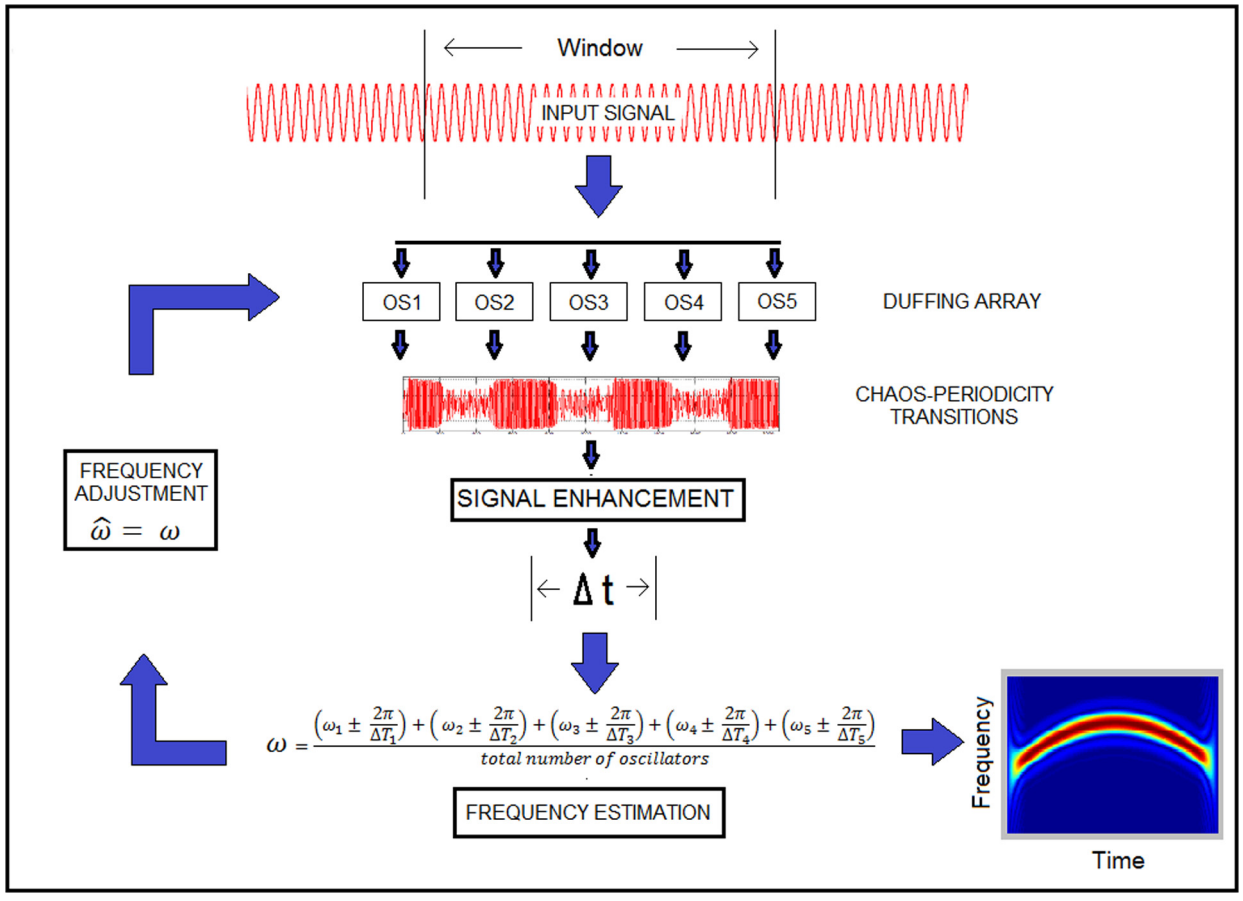

Fig. 9. Adaptive system (the time-frequency representation is generated after all the windows have been analyzed). (For interpretation of the colors in this figure, the reader is referred to the web version of this article.)

the system array adjusts the frequency according to the frequency found at each iteration, the system becomes adaptive.

As a direct result of the system being adaptive, the main advantage of the proposed method is that the signal frequency to be analyzed does not need to be either a linear or a quadratic chirp signal but it may have any general chirp rate of the form

$$y(t) = A \cdot \cos\left(\omega t + \dot{\omega} t^2 + \ddot{\omega} t^3 + \cdots + \omega^{(n)} t^n\right) \tag{10}$$

which implies that the signal may contain accelerations, decelerations or any variation that produces a change in its phase over time.

Fig. 9 is a schematic view which allows for a better understanding of how the entire system operates for such single chirp signals.

4.1. Time-frequency representation

This section describes how the time-frequency representation is obtained.

Because $\Delta\omega$ is calculated for each time window in which the unknown chirp signal was divided and because that particular window corresponds to a specific time then, the system array already gives one point in the TF representation. Since the system is adaptive, the next time window will have its corresponding time and $\Delta\omega$ which constitute again another point in the TF representation, and so on.

4.2. Adaptive Duffing array methodology

The proposed adaptive system array methodology is implemented as follows:

i. The chirp signal immersed in high levels of noise is presented for detection.
ii. Calculate window size in the time domain for a given expected error.
iii. Partition signal into corresponding n windows.
iv. nth window processing:
   a. set local frequency references for all OSj, $j = 1, \ldots, 5$ adjusted within a close variation of the most likely frequency estimate;
   b. the windowed chirp signal is presented to the 5 Duffing oscillator array;
   c. Signal Enhancement to OSj for $j = 1, \ldots, 5$;
   d. Measure Δt_i for all i-transitions at each OSj;
   e. ΔT_n average calculation;
   f. Estimate the instantaneous $\Delta\omega_n$;
   g. Save coordinate values for the Time vs. Frequency plot.
v. Update frequency reference for the nth $+1$ window.
vi. Recursive analysis for all windows.
vii. Generate TF representation.

The full algorithm is described in the flow chart presented in Fig. 10.

One interesting issue is that of evaluating the computational effort when using the proposed technique. Firstly, it is important to note that the program that implements the Adaptive Duffing System algorithm in fact converges and therefore it has an asymptotic behavior which, in turn, is given by the previously described main algorithm (Fig. 10). Then, it is easy to establish an upper bound by the use of the maximum rule [31] to the whole algorithm. Because there are two loops in the main algorithm, such upper bound belongs to the $O(n^2)$. This places our adaptive system in the same order of difficulty as that of the general Cohen's class [32], particularly the Choi–Williams and the Multiform Tiltable Exponential Distribution when they compute their kernel with $O(n^2)$ operations [33,34]. This relative computational cost will be experimentally proven in the next section.

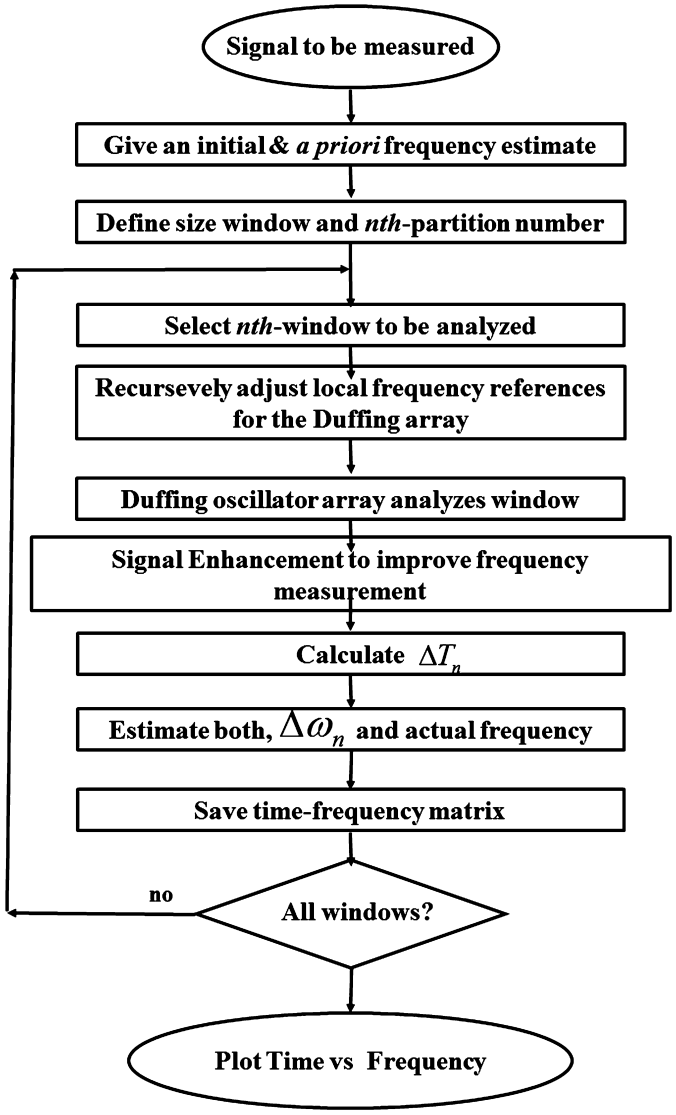

Fig. 10. Adaptive system algorithm.

5. Results

To verify that indeed the system operation is able to follow the frequency of a chirp input signal, simulations were performed in the absence and in the presence of noise, using a linear chirp and a quadratic chirp.

The frequencies used for the simulations were selected considering the frequency ranges at which some radar systems run. This was done to show the performance of the system with frequencies that can be found in real applications such as weather radar, air surveillance radar, tracking and ballistic missiles, among others [35,36].

5.1. Linear chirp

In this section all simulations were performed using linear chirp signals with additive noise $n(t)$ at different σ levels in agreement with the following equation:

$$y(t) = 0.5\cos\left[\left(6 \cdot 10^9\right)t + \left(45 \cdot 10^{13}\right)t^2\right] + \sigma \cdot n(t). \tag{11}$$

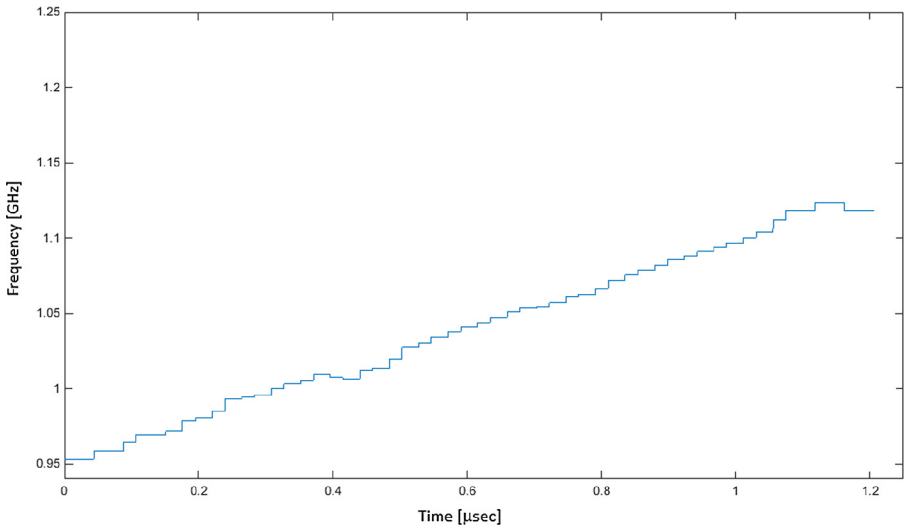

Fig. 11. Instantaneous frequency calculated with the Duffing system at 0 dB of SNR.

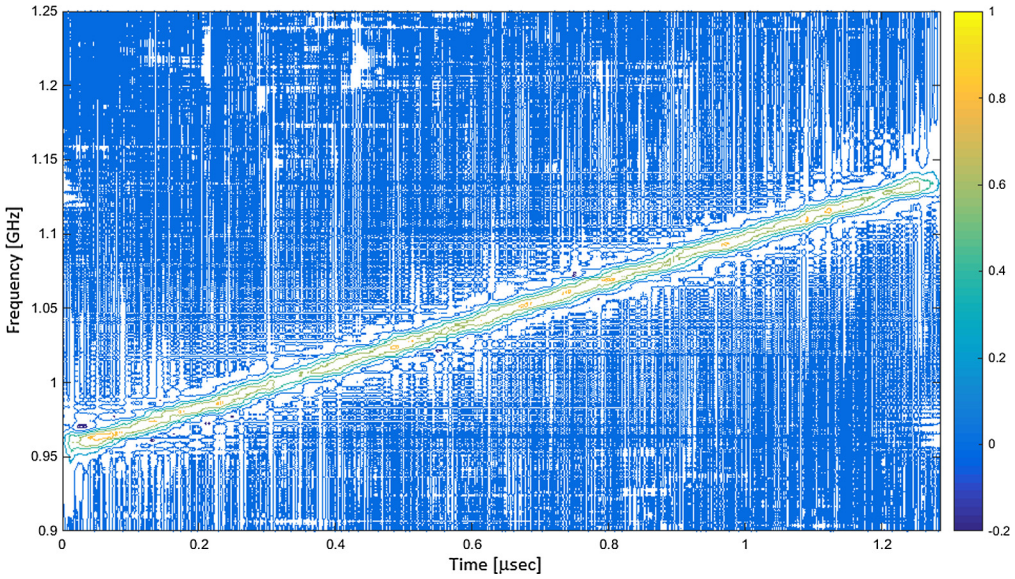

Fig. 12. Choi–Williams distribution; Linear chirp with 0 dB of SNR. (For interpretation of the colors in this figure, the reader is referred to the web version of this article.)

This signal has a frequency range that varies approximately from 950 MHz to 1.25 GHz.

For comparison purposes, the same chirp signal was analyzed by time-frequency methods that are commonly used with these types of signals, such as the Choi–Williams distribution and the MTED. These previous techniques performed well in our experiments at 0 dB of SNR but at higher noise levels, also worsened by the Doppler Effect, they all were severely affected and, therefore, all comparison experiments were done using this specific SNR.

5.1.1. Duffing system

The response of the Duffing oscillator system at 0 dB of SNR is shown in Fig. 11. It shows that although variations in the instantaneous frequency could be observed, the overall results indicate that the frequency estimation performed by the system is quite accurate and therefore a good TF representation. It is worth mentioning that during simulations for higher levels of noise, the response of the system gives, in general, reliable results.

5.1.2. Choi–Williams distribution (CWD)

The result for the CWD at 0 dB of SNR is shown in Fig. 12. Despite being able to estimate the instantaneous frequency, this method is affected by some components not desired in its TF representation (this effect is more noticeable when the noise is increased). It can be easily seen that, this method shows lower time-frequency resolution than the Duffing system (see Fig. 11).

5.1.3. Multiform tiltable exponential distribution (MTED)

This method, Fig. 13, detects the instantaneous frequency in a better way than the CWD, but continues to have lower time-frequency resolution than the Duffing system. The kernel applied for this kind of signal was the parallel strip form [18] as it gave the best experimental results.

5.2. Quadratic chirp

In this section, all simulations were performed with quadratic chirp signals in the presence of noise described by

$$y(t) = 0.5\cos\left[\left(5\cdot 10^{9}\right)t + \left(15\cdot 10^{14}\right)t^{2} - \left(98\cdot 10^{19}\right)t^{3}\right] + \sigma\cdot n(t). \tag{12}$$

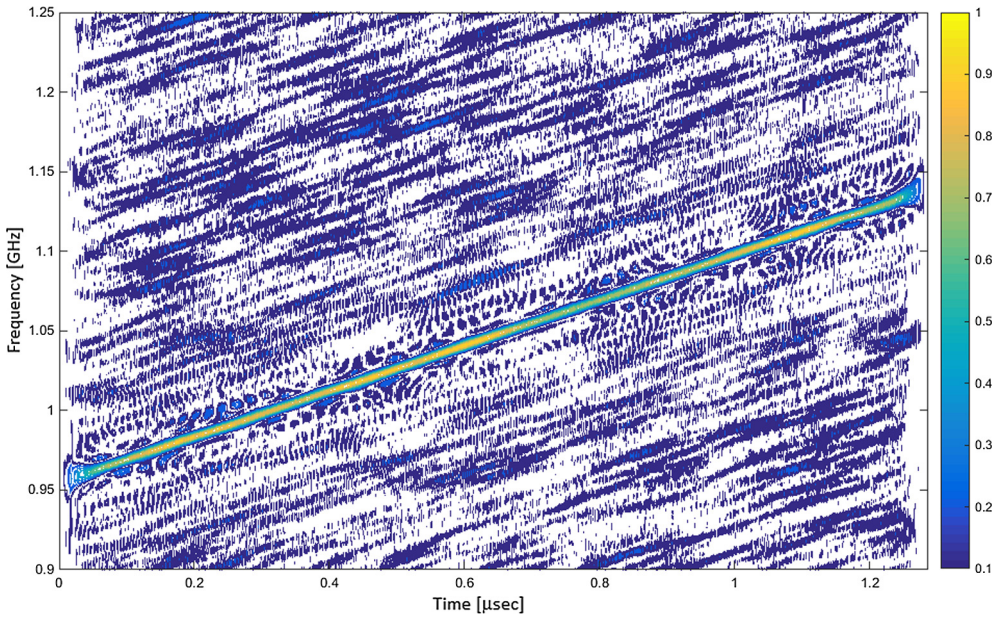

Fig. 13. MTED; Linear chirp with 0 dB of SNR. (For interpretation of the colors in this figure, the reader is referred to the web version of this article.)

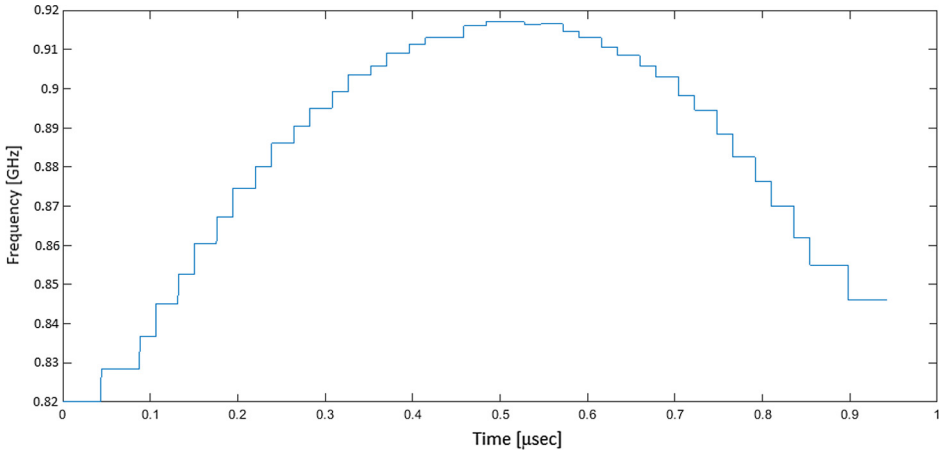

Fig. 14. Instantaneous frequency calculated with the Duffing system at 0 dB of SNR.

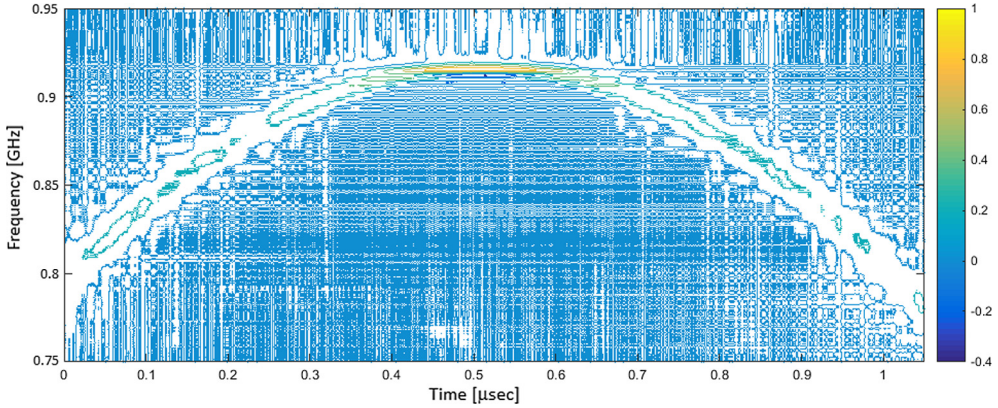

Fig. 15. Choi–Williams distribution; Quadratic chirp with 0 dB of SNR. (For interpretation of the colors in this figure, the reader is referred to the web version of this article.)

This signal covers a frequency range from 800 MHz up to 918 MHz approximately. Again, for comparison purposes, simulations from the proposed Duffing system are presented against the results from the same TF methods used at 0 dB of SNR.

5.2.1. Duffing system

Fig. 14 shows the instantaneous frequency estimation at 0 dB of SNR. Experiments were also performed for lower SNR indicating a great capability for detecting signals with a higher level of noise

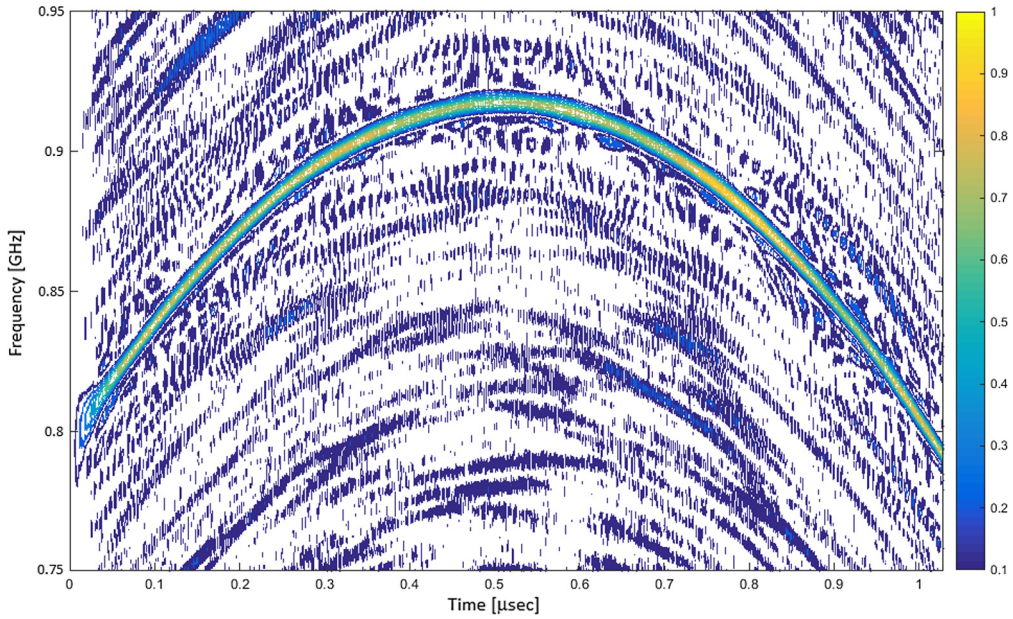

Fig. 16. MTED; Quadratic chirp with 0 dB of SNR. (For interpretation of the colors in this figure, the reader is referred to the web version of this article.)

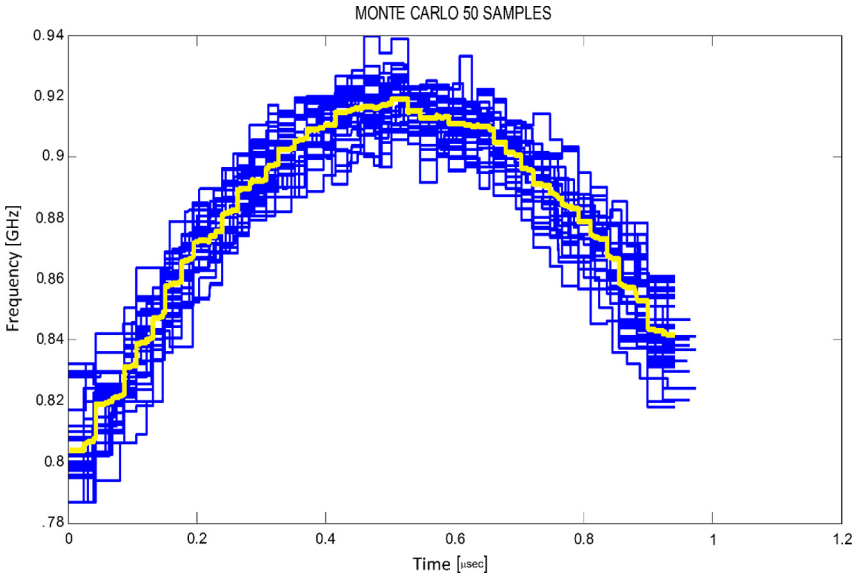

Fig. 17. Superimposed plots for Monte Carlo simulation (50 plots) and average estimated instantaneous frequency at −17 dB. (For interpretation of the references to color in this figure, the reader is referred to the web version of this article.)

as shown later in Fig. 18. It should be noted here that an overlapping heuristic window was used to obtain better time-frequency resolution.

5.2.2. Choi–Williams distribution

The first comparison is done against the CWD at 0 dB of SNR with the result presented in Fig. 15. The presence of cross terms generates errors in the estimation of the frequency which occurs mainly at the point of maximum curvature of the graph. For this case, like in the linear chirp case, a lower time-frequency resolution than the Duffing system is readily observed. Further, the CWD is affected by interference terms when the same frequency component appears at different periods of time [1,37].

5.2.3. Multiform tiltable exponential distribution (MTED)

Due to the lack of a kernel designed specifically for quadratic "chirp" signals, the *cross form* kernel [18] was used since such kernel presented the best results for the different simulations that were performed during the experiments. In the absence of noise, the MTED's performance is good since it does not present interference terms, and therefore the MTED can identify the fine frequency variation over time. Nevertheless, at 0 dB of SNR (Fig. 16) we can see that the time-frequency resolution decays and some undesired elements begin to appear. This method detects the instantaneous frequency in a better way than the CWD but continues to have a lower time-frequency resolution than the Duffing system.

Table 1
Relative errors among all different TF analysis techniques.

Method	Linear chirp error	Quadratic chirp error
Duffing	0.1771%	0.1866%
Choi–Williams	0.4533%	0.8143%
MTED	0.2844%	0.7835%

Finally, Table 1 shows the relative errors for each of the compared methods: Duffing, Choi–Williams distribution and MTED. Ab-

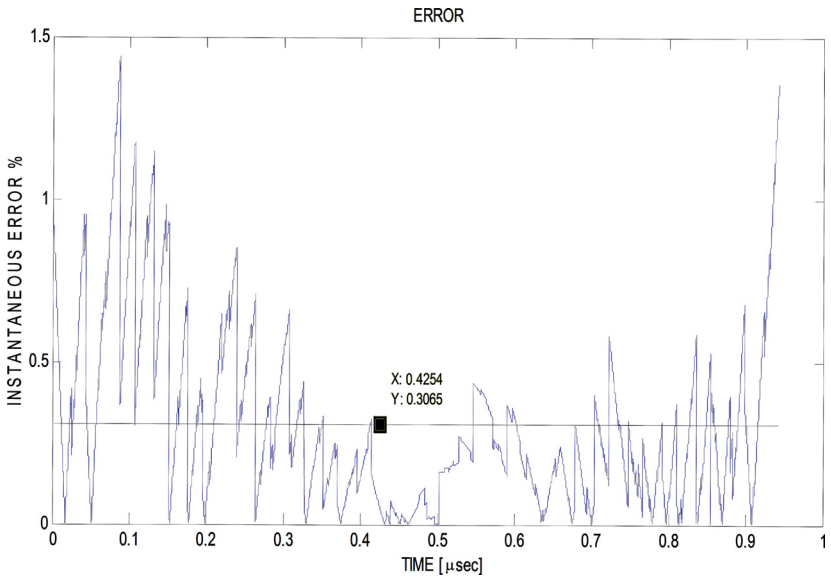

Fig. 18. Instantaneous % error and average error (constant line) = 0.3065%.

Table 2
Relative running time using the comparison TF techniques.

Method	Linear chirp [sec]	Quadratic chirp [sec]
Duffing	156	165
Choi–Williams	84	102
MTED	89	112

solute errors are calculated against the analytical expression for the frequency variations and the corresponding experimental result for each and all simulated TF methods and the MSE was used. It can be easily seen that the least relative errors for both linear and non-linear frequency variations, are those presented by the Duffing methodology.

Moreover, Table 2 shows the computational timing for each of the numerical tests performed with an Intel® Core i5 based computer, with 4 MB of RAM and running MATLAB® R2011a with 2^{12} chirp signal data length.

5.3. Monte Carlo simulation

The Duffing oscillator achieves excellent results in the presence of noise and it has been observed that it could measure a signal down to −28.5 dB SNR for the case of a constant frequency signal. During the experiments, simulations using chirp signals at different levels of noise were performed and good results were obtained. Hence, it was expected that the Duffing system would achieve good results with high levels of noise.

To demonstrate the noise limits at which our system is able to run, the Monte Carlo method was applied. Simulations were exclusively performed using the quadratic chirp signal described by equation (11) since, by having higher frequency variation than the linear chirp case, the frequency estimation will exhibit higher error. However, the results are equally valid for linear chirp signals even considering worst SNR scenarios.

The quadratic chirp signal elapsed within 942.4 ns, with a minimum frequency of 795.8 MHz, a maximum frequency of 917.6 MHz and a sampling frequency of 15.92 GHz (100 Grad/sec) giving 15,000 samples. To make the frequency estimate, 50 simulations were done for two different SNRs, one at 0 dB and the other at −17 dB. The limiting level of detection was reached at −17 dB of SNR since at these frequency changes, the system does not give an accurate measurement of all the frequencies involved.

Monte Carlo simulations for −17 dB SNR are shown in Fig. 17 where all 50 runs are superimposed as well as the corresponding final average estimated instantaneous frequency.

From Fig. 18, it can be seen that the average error is 0.3065% which is extraordinarily good considering that for such a quite low SNR all studied TFRs fail to measure such frequencies.

Monte Carlo results are similar for 0 dB SNR with an average error as low as 0.1796% which can be considered good as was already discussed.

6. Conclusions

This work achieves a measurement methodology for chirp signals by means of an adaptive Duffing oscillator array. We have proposed a method which takes time windows from the signal of interest and uses the chaotic properties of the Duffing oscillator instead of time-frequency representations. The principal advantage of this technique is that chirp signals can be analyzed for a frequency that varies with time and at low levels of SNR. A collateral important contribution is the enhancement of the Duffing oscillator response achieved with the correlation between its reference signal and the response itself. We have demonstrated that the system is able to detect linear and quadratic frequency shifts and in general it could meet any kind of nonlinear frequency variation. The Duffing oscillator has favorable characteristics for the analysis of weak signals, which presents a clear advantage over the tested traditional time-frequency techniques.

As future work, there is the need to compare the proposed method against most modern TF techniques such as the Compact Kernel distribution and adaptive time-frequency distribution [38]. Further, much extra work still needs to be done to test the performance of the Adaptive Duffing Array under multi-signaling conditions.

Acknowledgments

Carlos Bermudez-Gomez and Maribel Tello-Bello wish to thank the Mexican Council for Science and Technology (CONACYT) for financial support through the 374935 and 9613001 scholarships.

Carlos Bermudez-Gomez wishes to thank the Department of Electrical and Computer Engineering at the University of Massachusetts Dartmouth for its hospitality during the spring 2012 semester under the sponsorship of Dr. Antonio H. Costa.

References

[1] B. Boashash, Time Frequency Signal Analysis and Processing: A Comprehensive Reference, Elsevier, 2003.
[2] W.Z. Nie Chunyan, Application of chaos in weak signal detection, in: Measuring Technology and Mechatronics Automation, Shangshai, 2011, pp. 528–531.
[3] L.Q. Tao Huang, Chaos theory based ultrasonic Doppler for velocity measurement of fluid in the petroleum channel, in: Fifth International Conference on Natural Computation, Tianjin, 2009, pp. 460–463.
[4] X.W. Tao Xie, Noise immunity analysis in external excitation chaotic oscillator detecting system, in: International Conference on Intelligent System Design and Engineering Application, 2010, pp. 1013–1016.
[5] L. Tian-Liang, Frequency estimation for weak signals based on chaos theory, in: International Seminar on Future Biomedical Information Engineering, 2008, pp. 361–364.
[6] S.Z. Changjian Deng, The weak signal detection based on chaos and genetic algorithms, in: Second International Symposium on Information Science and Engineering, 2009, pp. 579–582.
[7] S.W. Deng Chen, The method for pulse wave velocity measurement based on chaotic oscillator, in: International Conference on Artificial Intelligence and Computational Intelligence, 2009, pp. 340–344.
[8] A.M.Y.K. Diallo Ouateni, Melnikov analysis of chaos in an epidemiological model with almost periodic incidence rates, Appl. Math. Sci. (2008) 1377–1386.
[9] J.T.H.Y. Chen, Chaos weak signal detecting algorithm and its application in the ultrasonic Doppler bloodstream speed measuring, in: 7th International Symposium on Measurement Technology and Intelligent Instruments, J. Phys. Conf. Ser. 13 (2005) 320–324.
[10] Y.C. Huang Yiran, A method of 2FSK signal detection using Duffing oscillator, in: ISECS International Colloquium on Computing, Communication, Control and Management, 2008, pp. 510–513.
[11] M.B.L. Galleani, Analysis of chaotic signals in the time frequency plane, in: Proc. IEEE Int. Symp. Time-Frequency and Time-Scale Analysis, 1994, pp. 357–360.
[12] C. Bermúdez-Gómez, R. Enriquez-Caldera, J. Martínez-Carballido, Chirp signal detection using the Duffing oscillator, in: 22nd Conference on Electronics, Communications and Computing, 2012, pp. 344–349.
[13] L. Debnath, Wavelet Transform and Their Applications, Birkhäuser, Texas, 2002.
[14] S. Mallat, Wavelet Tour of Signal Processing, 2nd ed., Elsevier, USA, 1999.
[15] C. Valens, A really friendly guide to wavelets, http://www.polyvalens.com, 2004.
[16] Z.L. Bo Le, Chaotic oscillator and other techniques for detection of weak signal, IEICE Trans. Fundam. E88-A (10) (2005) 2699–2701.
[17] D.Z. Fengli Wuan, Chaotic oscillator detection based on empirical mode decomposition and its application, in: International Workshop on Chaos-Fractals Theories and Applications, 2009, pp. 318–322.
[18] G. F-B, Antonio H. Costa, Design of time-frequency representations using a multiform, tiltable exponential kernel, IEEE Trans. Signal Process. 43 (10) (1995) 2283–2301.
[19] C. Li, Study of weak signal detection based on second FFT and chaotic oscillator, Nat. Sci. 3 (2) (2005) 59–64.
[20] F.H. Abolfazl Jalilvand, The application of Duffing oscillator in weak signal detection, ECTI Trans. Electr. Eng. Electron. Commun. 9 (1) (2011).
[21] P.W. Liqun Shen, The application of Melnikov function in weak signal detection with Duffing oscillators, in: The 2nd International Conference on Intelligent Control and Information Processing, 2011, pp. 854–858.
[22] G. Elert, Hypertextbook, 5 Abril de 2012, http://hypertextbook.com/chaos/43.shtml.
[23] M. Li-xin, Weak signal detection based on Duffing oscillator, in: International Conference on Information Management, Innovation Management and Industrial Engineering, 2008, pp. 430–433.
[24] I. Kovacic, M.J. Brennan, The Duffing Equation, Nonlinear Oscillators and Their Behavior, Wiley, 2011.
[25] P.J. Rober Grover Brown, Introduction to Random Signals and Applied Kalman Filtering, John Wiley & Sons, 1985.
[26] A. Rosado Muñoz, Las transformadas tiempo-frecuencia, in: A. Rosado Muñoz (Ed.), Desarrollo de técnicas de detección de fibrilación ventricular basadas en algoritmos Tiempo-Frecuencia, 1999, pp. 21–237.
[27] T.S.S. Rao Jammalamadaka, Higher order cumulants of random vectors and applications to statistical inference and time series, Indian J. Stat. 68 (2) (2006) 326–356.
[28] A. Swami, J.M. Mendel, C.L. Nikias, Higher-Order Spectral Analysis Toolbox User's Guide for use with MATLAB, 2001.
[29] Y.L. Ye Yuang, Study on EEG time series based on Duffing equation, in: International Conference on BioMedical Engineering and Informatics, 2008, pp. 516–519.
[30] Maribel Tello Bello, Rogerio Enriquez Caldera, Carlos Rodolfo Bermúdez Gómez, Doppler signal precise detection using an array of Duffing oscillators, in: International Conference on Waves in Science and Engineering, WISE 2013, 2013.
[31] G. Brassard, P. Bratley, Fundamentals of Algorithmics, Prentice Hall, 2011.
[32] B. Boashash, Time-Frequency Signal Analysis – Methods and Applications, Wiley Halsted Press, 1992.
[33] K.B. Hollinger, Code optimization for the Choi–Williams distribution for ELINT applications, Master in Science Thesis Degree in Electrical Engineering Naval Postgraduate School, Monterey, California, 2009.
[34] R.G. Barianuk, D.L. Jones, Optimal kernels for time-frequency analysis, in: Adv. Signal-Process. Algorithms Archit. Implement., vol. 1348, SPIE, 1990, pp. 181–187.
[35] C. Wolff, Radar tutorial, http://www.radartutorial.eu/07.waves/was04.en.html, 2012.
[36] www.mathworks.com.
[37] F. Hlawatsch, G.F. Boudreaux-Bartels, Linear and quadratic time-frequency signal representation, IEEE Signal Process. Mag. (1992) 21–67.
[38] B. Boashash, N.A. Khan, T. Ben_Jabeur, Time-frequency features for pattern recognition using high-resolution TFDs: a tutorial review, Digit. Signal Process. 40 (2015) 1–30.

Antonio H. Costa received the Ph.D. degree in electrical engineering from the University of Rhode Island, USA, in 1994. He also obtained the M.S. degree in electrical engineering and the B.S. degree (*summa cum laude*) in electrical engineering, computer engineering, computer science, and mathematics (quadruple major) from the University of Massachusetts Dartmouth (formerly Southeastern Massachusetts University), USA in 1985 and 1983, respectively. He joined the University of Massachusetts Dartmouth in September 1985, where he is now Chairperson and Professor of Electrical & Computer Engineering. From 2005 to 2007 he was Dean of the College of Engineering and from 2002 to 2005 he was Chairperson of the Department of Electrical and Computer Engineering. His current research interests are in the areas of signal and image processing with emphasis on nonlinear and time-varying signal processing and time-frequency methods.

Rogerio Enriquez-Caldera received the Ph.D. degree in electrical engineering from the University of New Brunswick, Canada, in 1994. He also obtained the M.S. degree in Applied Mathematics and Theoretical Physics from The University of New Brunswick, Canada in 1989 and the B.S. degree in Physics from the Universidad Nacional Autonoma de Mexico (UNAM) in 1984. He worked for the Astronomy Institute of UNAM from 1980 to 1988. From 1994 to 2000 he was Professor in Computer Science at ITESM, Mexico. He joined the National Institute for Astrophysics, Optics and Electronics in September 2000, where he was in charge of the technology office for the Large Millimeter Telescope until 2007. His actual areas of research are GPS signal processing, astronomical instrumentation, geomatics, and just very recently Science and Technology for Space where he is in charge of the Modeling, Simulation and Formation Flying Lab.

Maribel Tello-Bello is a doctoral student from Electronics Department in the National Institute of Astrophysics, Optics and Electronics (*INAOE*), 2014–2016. From 1998 to 2014 she was professor–researcher of Electronics and Computer Engineering Institute of Universidad Tecnológica de la Mixteca in Oaxaca, Mexico. She obtained the M.S. degree in Optics from National Institute of Astrophysics, Optics and Electronics (*INAOE*) in 1998 and the Bachelor's degree in Electronic Engineering from Benemerita Universidad Autonoma de Puebla (BUAP) in 1994.

Carlos Bermudez-Gomez received the M.S. degree in electrical engineering from the National Institute for Astrophysics, Optics and Electronics, Mexico in 2012. He obtained his B.S. degree in electrical engineering from the Santander University in Bucaramanga Colombia in 2000. He was Antonio Costa´s research assistant at the University of Massachusetts Dartmouth in 2012. He works as a Resident Engineer at Proctek LTDA (Process Control Technologies) in Colombia.